

# Efficacy of Electrically-Polarized 3D Printed Graphene-blended Spacers on the Flux Enhancement and Scaling Resistance of Water Filtration Membranes

Numan Yanar, Eunmok Yang, Hosik Park, Moon Son,\* and Heechul Choi\*

Cite This: *ACS Sustainable Chem. Eng.* 2021, 9, 6623–6631

Read Online

ACCESS |



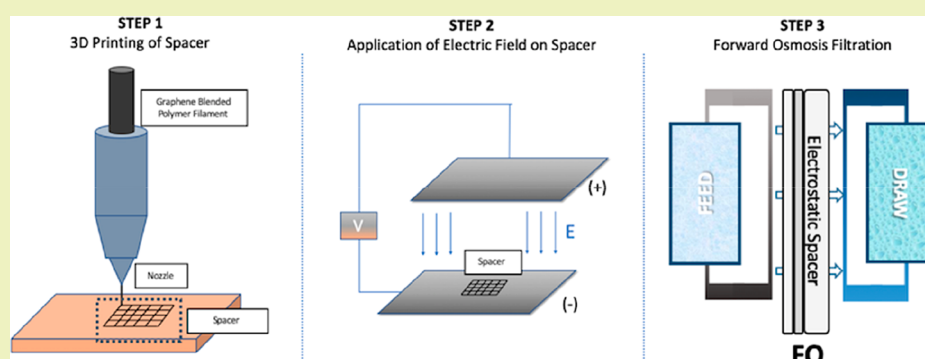
Metrics &amp; More



Article Recommendations



Supporting Information



**ABSTRACT:** In this research, an electrically polarized graphene-poly(lactic acid) (E-GRP) spacer is introduced for the first time by a novel fabrication method, which consists of 3D printing followed by electrical polarization under a high voltage electric field (1.5 kV/cm). The fabricated E-GRP was tested in an osmotic-driven process (forward osmosis system) to evaluate its performance in terms of water flux, reverse solute flux, and ion attraction compared to a 3D printed nonpolarized graphene-poly(lactic acid) (GRP) spacer and a poly(lactic acid) (PLA) spacer. The use of the developed E-GRP as a draw spacer showed >50% water flux enhancement ( $32.4 \pm 2$  Liter/m<sup>2</sup>/h (LMH)) compared to the system employing the GRP ( $20.5 \pm 2.3$  LMH) or PLA ( $20.8 \pm 2.1$  LMH) spacer. This increased water flux was attributed to the increased local osmotic pressure across the membrane surface due to the ions adsorbed by the polarized (E-GRP) spacer. As a feed spacer, the E-GRP also retarded the gypsum scaling on the membrane compared to the GRP spacer due to the dispersion effect of electrostatic forces between the gypsum aggregation and negatively charged surfaces. The electric polarization of the E-GRP spacer was shown to be maintained for >100 h by observing its salt adsorption properties (in a 3 M NaCl solution).

**KEYWORDS:** electrostatic spacers, graphene spacers, membrane filtration, 3D printing, membrane scaling, forward osmosis

## INTRODUCTION

Water scarcity has been a critical problem in the last few decades due to drought accelerated by global warming.<sup>1</sup> As fresh water resources are already limited, the need for treating nonpotable waters has emerged.<sup>2</sup> As of 2020, we are confronting a global pandemic and its indirect side effects, one of which is the mixing of viruses with water.<sup>3–5</sup> Although the United States Environmental Protection Agency stated that drinking water is still safe for drinking,<sup>6</sup> Casanova et al. stated that coronaviruses can remain infectious in water for days to weeks.<sup>7</sup> Since we are faced with this critical situation that is endangering human lives, virus-selective water treatment methods come to the front compared to other treatment methods. When virus-selectivity is a concern, membrane-treatment methods can be considered the primary approach due to their excellent selectivity of water over other matter.<sup>8</sup> For the success of the membrane process to secure clean water,

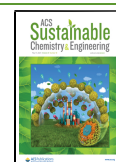
the membrane's performance should be maintained with minimal changes in energy consumption over long-term operation; however, most studies have focused on the development of novel membranes<sup>9,10</sup> and are already at their limit for the current technology.<sup>11</sup> In addition, other parts of the membrane processes should also be further developed to increase the overall efficiency of the membranes processes.

The development of the channel spacer is one of the most critical parts affecting the performance of the membrane process as it distributes the feedwater stream and works as a

**Received:** December 28, 2020

**Revised:** April 17, 2021

**Published:** May 3, 2021



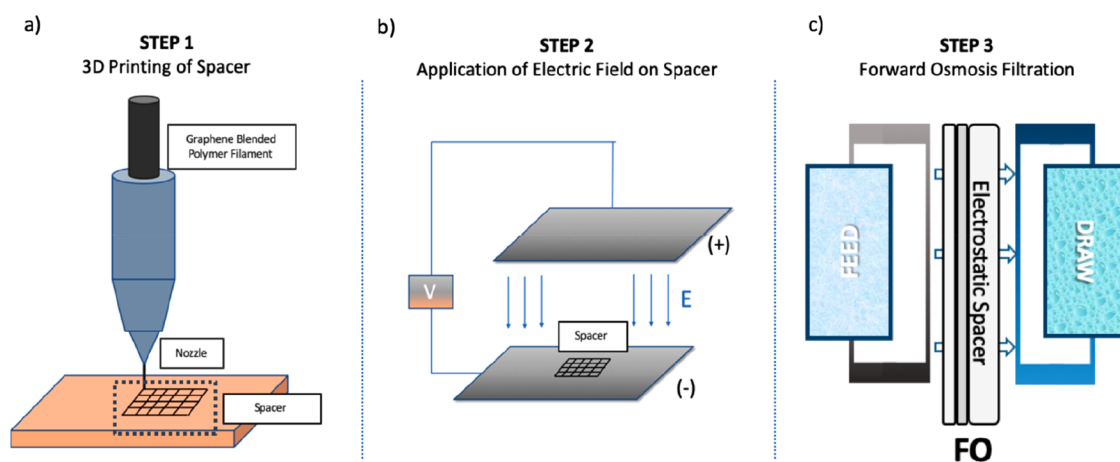


**Figure 1.** Fabrication and application processes of the electrostatic graphene-blended PLA spacers (E-GRP): a) 3D printing, b) electric polarization, and c) forward osmosis filtration.

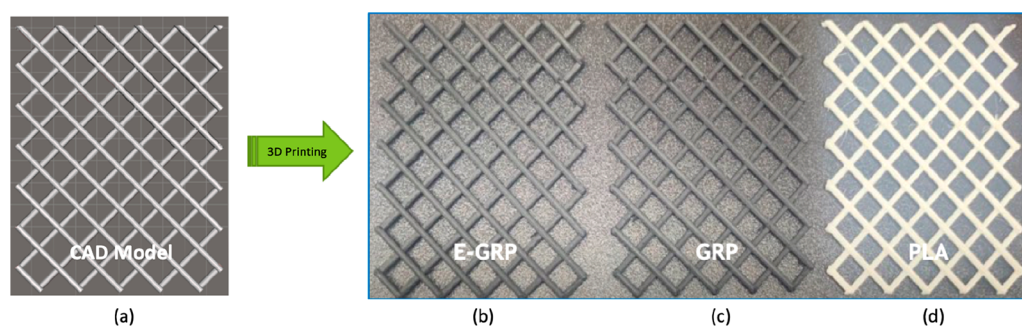


**Figure 2.** a) The CAD model and the fabricated b) E-GRP, c) GRP, and d) PLA spacers.

protective guard to the membrane surface.<sup>12</sup> To date, most studies on spacers have been conducted by computer modeling with a focus on the shape of the spacers.<sup>11</sup> There are relatively few investigations using in situ filtration tests, although computational fluid dynamics (CFD) modeling of the geometry has been extensively performed.<sup>13–16</sup>

The fabrication material, surface structure, and functionality of spacers also carry great importance. In this regard, Yanar et al. compared the performances of acrylonitrile butadiene styrene (ABS), polylactic acid (PLA), and polypropylene (PP) as the spacer materials by employing them in a forward osmosis (FO) type membrane filtration system and clearly observed differences in fouling and ion attraction by the spacers.<sup>17</sup> On the other hand, there have been a lot of studies on different types of coatings for spacers to enhance their surface properties. Some examples of such studies are a nanosilver surface modification to a reverse osmosis (RO) membrane and a spacer for mitigating biofouling,<sup>18</sup> an antibacterial spacer obtained by the sonochemical deposition of ZnO nanoparticles,<sup>19</sup> nanosilver-modified feed spacers for antibiofouling of ultrafiltration (UF) membranes,<sup>20</sup> a polyaniline and polypyrrole (PPy) coating onto a stainless steel grid for high selectivity oil–water separation,<sup>21</sup> graphene coating on a steel mesh for oil/organic-water separation,<sup>22</sup> and the formation of nanotubes on stainless steel meshes by electropolymerization.<sup>23</sup> Nevertheless, surface coating has not always been successful at enhancing the spacer performance. For example, polydopamine, polydopamine-g-PEG, and copper coatings on feed spacers did not show a high performance in mitigating biofouling.<sup>24,25</sup> Similarly, CuO modified spacers also

did not improve the performance of RO systems in terms of biofouling.<sup>26</sup>

Alternative techniques based on electrochemistry have been applied to filtration systems to enhance the overall performance regarding water flux and fouling resistance. Self-cleaning was first demonstrated in electrically conductive titanium meshes used as spacers for microfiltration (MF).<sup>27</sup> The electric polarization of a spacer has also been utilized to enhance the performance of water filtration membranes. An electrically polarized titanium mesh was used for biofouling control in an RO system.<sup>28</sup> The effect of electrical polarization on the movement of ions in water and on membrane systems has been investigated by a variety of studies. Kim et al. introduced the effect of electric field on the mitigation of salt ions and showed that it also reduces the internal concentration polarization (ICP).<sup>29</sup> Son et al. investigated the ion migration induced by an electrical field on the water flux in an FO process by using a thin-film composite (TFC) membrane. This research showed that the electric field that brings protons closer to the membrane surface can provide enhanced osmotic pressure due to the high localized concentration of protons.<sup>30</sup> When functionalized graphene nanosheets were used as a membrane, a faster movement of the salt ions under the electric field was also reported.<sup>31</sup>

In this research, we propose an electrically polarized graphene-blended (E-GRP) spacer as a salt adsorber prepared by 3D printing followed by a polarizing step (Figure 1a and b). 3D printing is a versatile fabrication method, which allows to control the size, scale, and material of the final product.<sup>16,32–34</sup> As the ion movement (or concentration) and electric

polarization on the draw side are crucially important in the FO process, the developed E-GRP spacer was employed on the draw side to investigate the changes in FO performance (Figure 1c). We also employed E-GRP on the feed side of the membrane by filtrating a feed solution with organic salts to check its performance for the mitigation of membrane surface scaling. To our knowledge, this is the first attempt to fabricate an electrically polarized conducting spacer and apply it to a membrane process.

## MATERIALS AND METHODS

The spacers were designed with the same filament thickness of 50 mil (1.27 mm) spacers with a pore size four times larger than that of commercial spacers (Figure S1). The reason for the enlarged size parameters was to allow the membrane to have a larger osmotic concentration area and to avoid the precision limitations of Fused Deposition Modeling (FDM) 3D printers. A Computer Aided Design (CAD) model of the spacer with dimensions 45 mm × 60 mm × 1.905 mm was prepared using Autodesk Meshmixer and Blender (Figure 2).

For the 3D printing of the samples, we utilized an FDM 3D printer (OpenCreators-Almond, Republic of Korea) (Figure 1a), since it allows the freedom to choose the printing materials as opposed to other types of 3D printers. The fabricated PLA, graphene-blended PLA (GRP), and E-GRP were expected to have the same geometry, as the same printing procedure was applied. For the pristine PLA spacer, 1.75 mm of natural PLA filaments (PLABS, Republic of Korea) were used. For the GRP and E-GRP spacers, we utilized 1.75 mm of conductive graphene blended PLA filaments with an 8% graphene/PLA ratio and a volume resistivity of 0.6 Ohm-cm<sup>35,36</sup> (Graphene Laboratories, United States). The more amount of graphene blending would result in huge amount of high dielectric loss, which would result in lower electric polarization capacity.<sup>37</sup> High dielectricity of graphene provides high electric polarization capacity.<sup>38</sup> High insulating properties of PLA is considered to wrap graphenes for keeping the electret property for longer time.<sup>39</sup>

After the printing procedure, the spacers were washed first with ethyl alcohol and then with deionized (DI) water with the resistivity of 18.2 mΩ-cm at 25 °C.<sup>40</sup> An ultrasonicator (B8510-MT, Branson, USA) was used to remove the remaining filament particles from the spacers.

After the spacers were dried, one of the graphene-PLA spacers was placed into a lab-scale electric field system consisting of two parallel-plates at a distance of 20 cm. We subsequently applied ±15 kV between the plates for 2 h to electrically polarize the GRP spacer to obtain an E-GRP one. The electric field was calculated with the following formula:<sup>41</sup>

$$E = \frac{\Delta V}{d} \quad (1)$$

where E is the electric field (V/cm), ΔV is the potential difference between the plates (V), and d is the distance between the plates (cm).

The surface charge densities of graphene spacers were also measured. Two flat graphene/PLA samples with an area of 3 cm × 1.5 cm and a thickness of 200 μm were fabricated. One of these samples was electrically polarized for 2 h in the same electrical field conditions above. Then, the zeta potentials of the samples were measured to calculate the surface charge densities using the Graham equation:

$$\sigma = \sqrt{8\epsilon_r\epsilon_0kTI} \sinh\left(\frac{ze\zeta}{2kT}\right) \quad (2)$$

where σ is the surface charge density, which is the hyperbolic function of the measured zeta potential ζ. I is the total electrolyte concentration, ε<sub>0</sub> is the vacuum permittivity, which is 8.854 × 10<sup>-12</sup> F·m<sup>-1</sup>, ε<sub>r</sub> is the relative dielectric permittivity of the solvent, e is the elementary charge, equal to 1.602 × 10<sup>-19</sup> C, kT is the thermal energy (k is the Boltzmann constant, which is 1.381 × 10<sup>-23</sup> J·K<sup>-1</sup> and T is

the temperature in Kelvin), and z is the ion valence.<sup>42</sup> For a 0.6 M NaCl solution, ε<sub>r</sub> can be calculated as follows:

$$\epsilon_r = \epsilon_w + 2\bar{\delta}c \quad (3)$$

where ε<sub>w</sub> is the dielectric permittivity of water, which is 78.2 at 25 °C<sup>43</sup> and δ̄ represents the relative contributions of the two ions in a single case (δ̄ =  $\frac{\delta^+ + \delta^-}{2}$ ). The value of δ<sup>+</sup><sub>Na+</sub> was taken as -8, δ<sup>-</sup><sub>Cl-</sub> as -3, which led to δ̄ being equal to -5.5. Finally, c is the concentration of the solution.<sup>44</sup>

The Debye length in the NaCl electrolyte solution is also considered to observe the effect of electrolyte concentration for solid charge carrier's net electrostatic effect.

$$\lambda_D = \sqrt{\frac{\epsilon_r\epsilon_0kT}{\sum_i \rho_{\text{ooi}} e^2 z_i^2}} \quad (4)$$

where ρ<sub>ooi</sub> is the number density of ion type i and z<sub>i</sub> is the ion valency.<sup>45</sup>

In order to observe the relative osmotic change on the membrane surfaces regarding to its distance to the electrically polarized spacer filament, we placed physically attached membrane-spacer couples (spacers on the draw side of membranes) of GRP and E-GRP for 12 h to the bottom of 300 mL glass beakers filled with 0.6 M NaCl solution (Figure S2a). After 12 h, membrane-spacer couples are dried, and concentrated salt volumes on the middle parts of three designated zones (Figure S2b) of the membrane surfaces were measured with an x-y scanning distance of 500 μm at 10 steps by using a Surface Nanoprofiler (Nanomap-D/Alpha-steps, HTSK, Gyeonggi, Korea). It should be noted that average surface volume of the pristine membrane is extracted from the results to obtain net values.

The thickness of each spacer was first characterized at the millimeter scale by a scanning field emission electron microscope (FE-SEM, S-4700 Hitachi, Japan). The junction points of the spacers were also visualized to ensure that intermembrane spaces were provided. SEM images were also taken for the surfaces of polarized and nonpolarized flat graphene blended PLA samples to observe if electric polarization creates any surface integrity change.

As we proposed these spacers for its ion attraction and for employing in a forward osmosis system, we applied it first on the draw side, where a highly concentrated sodium chloride (NaCl) solution is used. For comparison, the spacer was also tested on the feed side.

A forward osmosis system with an effective membrane area of 19.35 cm<sup>2</sup> and a total effective height of 2.6 mm was used in the cross-flow mode with a flow velocity of 200 cm<sup>3</sup>·min<sup>-1</sup> on both the feed and draw sides. A commercially available woven permeate spacer and commercial FO membranes extracted from an FO module (Toray Korea) were used in AL-FS (active layer facing feed side) orientation to test the performance of the system (Figure 1).

For the case where the driving force was the osmotic pressure across the membrane, a 0.6 M NaCl solution (draw solution) was paired with DI water (feed solution). The water weight and electrical conductivity on the feed side were automatically recorded by a computer every minute. Filtration tests were conducted for 1 h for each sample once the system was stabilized (i.e., stable water flux). The water flux, J<sub>w</sub>, and the reverse solute flux, J<sub>s</sub>, were calculated as given below:

$$J_w = \frac{V}{A_m \Delta t} \quad (5)$$

$$J_s = \frac{V C_t - V_0 C_0}{A_m t} \quad (6)$$

where J<sub>w</sub> is the water flux, V is the volume of filtrated water (L), A<sub>m</sub> is the effective membrane area of the testing module, and Δt is the permeation time (h).<sup>46,47</sup> The reverse solute flux was obtained from the change in feed conductivity per minute and converted into g/m<sup>2</sup>/h (gMH). C<sub>t</sub> (g·L<sup>-1</sup>) and V<sub>t</sub> (L) are the concentration and volume of the feed solution measured at time t, respectively, and C<sub>0</sub> (g·L<sup>-1</sup>) and

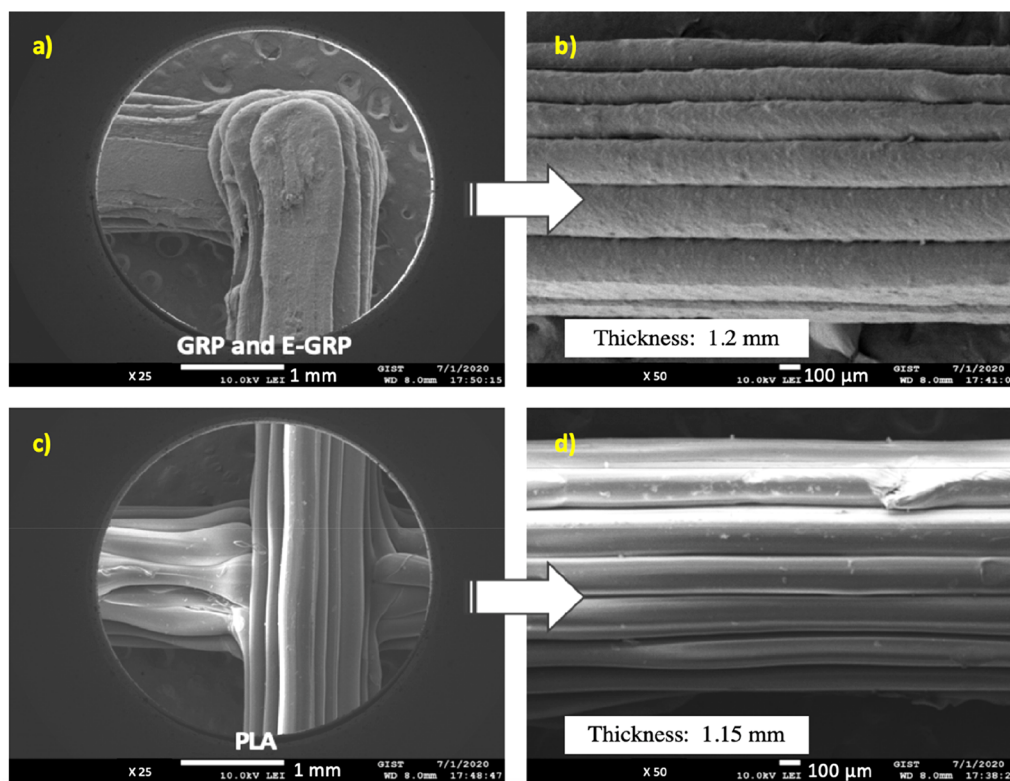


**Figure 3.** Top and cross-sectional SEM images of the a, b) GRP and E-GRP and c, d) PLA spacers.

$V_0$  (L) are the initial concentration and volume of the feed solution, respectively. The concentration values were determined from the solution conductivities.<sup>48</sup> Further the investigation was done by using 3 M NaCl solution (draw) paired with DI water (feed) for understanding the performances of spacers under highly concentrated draw concentrations. In order to confirm the polarization longevity of E-GRP in draw solution, 10 h flux declines of E-GRP and GRP are also compared while 3 M NaCl in draw side and DI water in feed side are used.”

The performance of E-GRP as the feed spacer was further tested by placing a feed solution containing inorganic salts—19 mM NaCl, 20 mM sodium sulfate ( $\text{Na}_2\text{SO}_4$ ), and 35 mM calcium chloride ( $\text{CaCl}_2$ )—and placing 0.6 M NaCl solution on the draw side. The solubility product of the  $\text{Ca}^{2+}$  and  $\text{SO}_4^{2-}$  concentrations in the feed solution was slightly higher (with a saturation index [SI] of 1.3), which can create gypsum scaling on the membrane at a reasonable flow rate, which was  $200 \text{ cm}^3 \cdot \text{min}^{-1}$  for this experiment, as stated above.<sup>49,50</sup>

To further understand the effect of electric polarization on the ion attraction on the spacers, the spacers were each placed in 300 mL of 3 M NaCl solution for 12 h. This procedure was done right after the E-GRP polarization for 100 h. After a 12 h deposition of  $\text{Na}^+$  and  $\text{Cl}^-$  ions on the spacers, each was first placed in a 300 mL beaker filled with DI water and then in an ultrasonicator for 1 h. The conductivity of each solution with the released ions was subsequently measured after removing the spacers. Next, the conductivities were converted into total dissolved solids (ppm) and osmotic pressure unit (bar).

$$P_{\text{osm}} = 1.19(T + 273) \sum (m_i) \quad (7)$$

In this formula,  $P_{\text{osm}}$  = osmotic pressure (in psi),  $T$  is the temperature (in °C), and  $\sum(m_i)$  is the sum of molal concentrations in the solution.<sup>51</sup>

The surface charge density in the 3 M NaCl solution was also calculated by taking  $\epsilon_r$  as 54.<sup>44,52</sup>

For the cost analysis of E-GRP, we obtained the business electricity prices<sup>53,54</sup> of top 12 countries according to latest available data from World Bank for Gross Domestic Product (GDP).<sup>55</sup> Actual power  $P$

(kW) is calculated from the following formulas. In here,  $S$  (kW) is the apparent power, P.F. (taken as 1) is the power factor (unitless) while  $V$  is voltage and  $I$  (A) is the current.

$$S = V \times I \quad (8)$$

$$P = S \times \text{P.F.} \quad (9)$$

Total consumed energy ( $E$ ) is calculated by multiplying actual power  $P$  with time  $t$  (time).

$$E = P \times t \quad (10)$$

By using actual power, 2 h price of used electricity for electric field production and 20 min price of used electricity for FDM type 3D printing machine are calculated for the spacer.<sup>56</sup> Material cost per  $\text{cm}^2$  spacer area is calculated by taking the gram price of graphene blended filament as reference which was 100 dollars for 100 g. In the end, total cost is indicated by summing up the electricity costs and the material cost (Minor costs such as transportation cost or postproceeding cost are ignored).

## RESULTS AND DISCUSSION

The 3D printed samples were successfully fabricated with marginal differences from the CAD model (Figure 2). The original design was 50 mil (1.27 mm) thick; however, the printed samples showed a relatively lower thickness due to the limited resolution of the layer by layer printing method of the FDM 3D printer. While the thicknesses of the GRP and E-GRP spacers were equal to 1.20 mm, that of the PLA spacer was 1.15 mm (<4% difference). It can be noticed that blending graphene increased the rigidity of the melted filament, which resulted in a relatively higher precision than for the PLA spacer without blending (Figure 3). Surface integrity of graphene-blended PLA spacer after and before polarization was also observed in order to see if electric polarization creates any change. However, we did not observe any visible change (Figure S3).

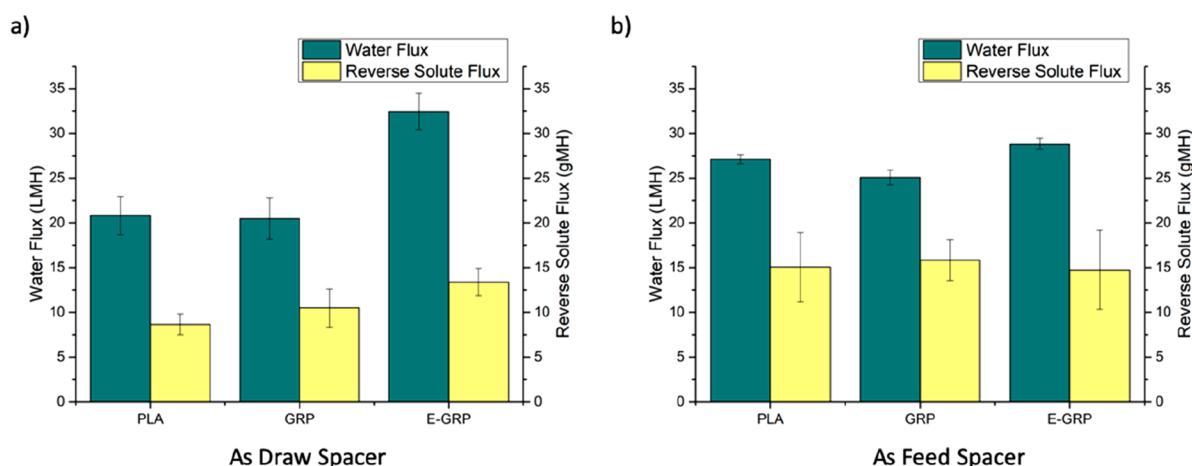


Figure 4. Pure water flux of each spacer on the a) draw side and b) feed side.

After the E-GRP was polarized under a calculated electric field of 1.5 kV/cm, the prepared spacers were first tested by placing them on the draw side, as our purpose was to analyze the effect of ion attraction on the spacers. When the E-GRP spacer was used as a draw spacer,  $32.4 \pm 2$  Liter/m<sup>2</sup>/h (LMH) of water flux (WF) and  $13.4 \pm 1.5$  gMH of reverse solute flux (RSF) were measured. This measured WF was higher than that of the PLA ( $20.8 \pm 2.1$  LMH) or GRP ( $20.5 \pm 2.3$  LMH) spacers (Figure 4a). Since the reverse solute flux is generally proportional to the water flux in the FO process, less solute permeation was observed for PLA ( $8.7 \pm 1.2$  gMH) or GRP ( $10.5 \pm 2.1$  gMH) compared to E-GRP. We explain this effect with the Gouy–Chapman theory, which states that there should be exactly balanced by an equal and oppositely charged ions or counterions in the solution adjacent to the charged surface and a deficit of similarly charged ions or co-ions.<sup>57</sup> Based on this, the interfacial potential at the polarized surface should increase the number of ions attached to it to an equal number of ions of opposite charge in the solution. Thus, the surface near to the spacer is expected to have a higher counterion concentration (Figure S4), which will also increase the local osmotic concentration, resulting in higher flux. To further understand this phenomenon, we calculated the surface charge density on the E-GRP and GRP spacers as a hyperbolic function of the surface zeta potential using the Grahame equation. As we were not able to measure the surface zeta potential of the spacers due to their shapes, we prepared 200  $\mu\text{m}$  flat samples from the same printing material and polarized one of them in the same conditions as the E-GRP spacer. From the measured zeta potentials, the calculated surface charge density of the E-GRP ( $-4.2$  mC/m<sup>2</sup>) spacer was found to be higher than that of the GRP ( $-0.27$  mC/m<sup>2</sup>) one (Figure S5). Therefore, the surface charge density was enhanced through the polarization of the graphene-blended spacer, an effect that could provide higher local osmotic concentration at the membrane surfaces near the polarized spacers. Furthermore, the collection of ions on the spacer reduced the external concentration polarization on the surface of the membrane. We also investigated the performances of spacers at draw side while high concentration draw solution (3 M NaCl) is used. When the E-GRP spacer was used,  $42.5 \pm 0.7$  LMH of WF and  $24.7 \pm 3$  gMH of RSF were measured. WFs for PLA and GRP were  $38.6 \pm 1.1$  LMH and  $37.5 \pm 0.8$  LMH, respectively. RSFs of PLA and GRP were observed as  $19 \pm 1.4$  gMH or  $20 \pm 2.1$

gMH, respectively (Figure S6). Compared to the performance at the draw solution of 0.6 M NaCl, flux increasing performance of E-GRP was relatively less at 3 M NaCl solution. This shows us that E-GRP is more efficient for lower concentration draw solutions (<3 M) such as seawater ( $\sim 0.6$  M). In this point, it should also be noted lower concentration draw solutions are more preferred for indirect desalination or water reuse applications, because (i) concentrates or brines contain high concentration of salts, and residuals of seawater pretreatment that can negatively affect the membrane performance; (ii) more efficient dilution of draw solution at the end of osmotic operation; (iii) lower cost of for the desalination of diluted draw solution as a result of using low pressure. Therefore, current seawater desalination plants are preferring to use seawater as draw solution rather than brines of concentrates.<sup>58</sup> Using E-GRP at lower concentration draw solutions will be beneficial to obtain the osmotic effect of higher concentration draw solutions by avoiding the drawbacks.

Further investigation was done by profiling accumulated salt volumes on the different zones of membrane surface after placing membranes with E-GRP and GRP in 0.6 M NaCl solutions for 12 h. The results showed that salt concentration on the membrane surface of E-GRP is proportionally increasing regarding to the distance of membrane surface to the electrically polarized spacer filament. When GRP was used, middle regions of designated A1, A2 and A3 zones of membrane surface had  $4626 \pm 1882$   $\mu\text{m}^3$ ,  $7015 \pm 2465$   $\mu\text{m}^3$  and  $8431 \pm 428$   $\mu\text{m}^3$  accumulated salt volumes, respectively (Figure S7a). These volumes were  $18607 \pm 4794$   $\mu\text{m}^3$  (A1),  $10332 \pm 630$   $\mu\text{m}^3$  (A2) and  $7767 \pm 1380$   $\mu\text{m}^3$  (A3) for the case of E-GRP (Figure S7b). These results show that local osmotic pressure on membrane surface is also proportional in macro scale to the distance of membrane surface from the filaments of electrically polarized spacer. When the results belonging to unpolarized GRP is seen, this kind of correlation was not found. Topographic images obtained from Surface Nano-Profiler can also be seen from Figure S8.

Flux decline of GRP and E-GRP for 10 h for was also observed in order to understand if there is any loss in the performance of E-GRP. However, similar flux declines were observed for both polarized and nonpolarized spacers (Figure S9).

The effect of using E-GRP as a feed spacer was also investigated (Figure 4b). On the feed side, E-GRP (WF:  $28.8 \pm 0.6$  LMH and RSF:  $14.7 \pm 4.4$  gMH) had a performance similar to GRP (WF:  $25.1 \pm 0.8$  LMH and RSF:  $15.8 \pm 2.25$  gMH) and PLA (WF:  $27.1 \pm 0.5$  LMH and RSF:  $15 \pm 3.8$  gMH). As there were no ions present in the feed solution, the E-GRP spacer was not able to adsorb ions; thereby, only marginal changes in the water flux and reverse solute flux were found.<sup>59</sup>

Ion adsorption and desorption capacities of each spacer were further investigated by measuring the amount of collected ions on E-GRP, GRP and PLA by dipping in 3 M NaCl solutions (Figure S10). E-GRP clearly showed the greater amount of collected ions on it compared to PLA and GRP spacers. E-GRP collected  $129,000 \pm 3650$  ppm ions ( $100 \pm 2.8$  bar in terms of osmotic pressure) on it during 12 h dipping right after the polarizing, whereas it decreased to  $106,000 \pm 3500$  ppm 100 h after polarization ( $82 \pm 2.7$  bar in terms of osmotic pressure). In contrast, GRP had  $92,450 \pm 450$  ppm ( $72 \pm 0.3$  bar in terms of osmotic pressure), while PLA had  $73,700 \pm 1150$  ppm ( $57 \pm 0.9$  bar in terms of osmotic pressure) as average (Figure 5). Thus, the effect of electrostatic forces on

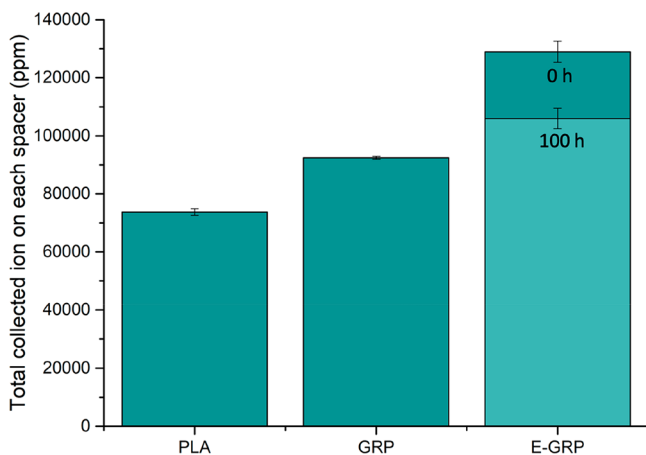


**Figure 5.** Total collected ion on each spacer right after and 100 h after electric field application to E-GRP.

the collection of ions on spacers instead of the membranes could be expected. In order to support this data, surface charge densities of E-GRP ( $-7.4$  C/m<sup>2</sup>) and GRP ( $-0.53$  C/m<sup>2</sup>) were also calculated for 3 M NaCl solution from Grahame Equation (Figure S11). It shows that surface charge densities are increasing with the increasing solvent concentration, which also affect total collected ions on spacer surfaces. Therefore, E-GRP's superior ion adsorption capacity was proportionally increased to the solvent concentration. Although relatively thin Debye length of 4.61 nm for 3 M NaCl was calculated, it was also previously studied that the Debye length is not applicable for higher solvent concentrations of  $>0.1$  M as it does not also consider the effect of surface charges of the solid surface.<sup>60,61</sup>

E-GRP as a feed spacer was further tested to observe the scaling performance, when the feed was concentrated with inorganic salts of NaCl, Na<sub>2</sub>SO<sub>4</sub>, and CaCl<sub>2</sub>. The use of the E-GRP as a feed spacer has suppressed the gypsum scaling on the membrane surface at the feed side. Only ~20% of flux reduction was found for E-GRP, whereas  $>80\%$  of water flux was declined for the pristine GRP during 4 h of operation (Figure 6). This improved gypsum scaling resistance of the E-

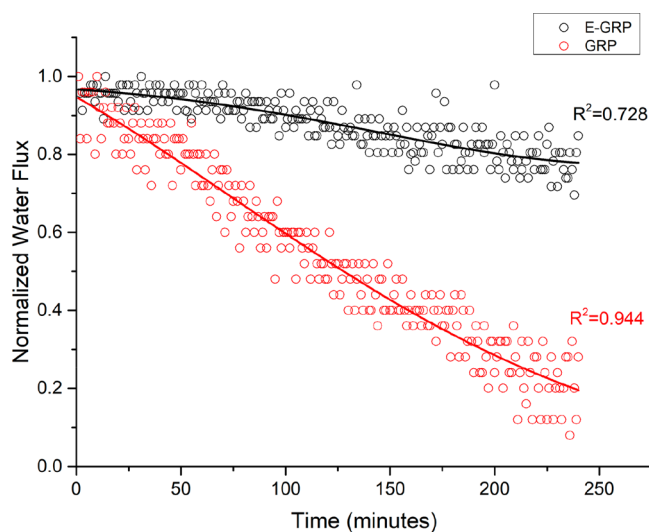


**Figure 6.** Normalized Water Flux for 4 h gypsum scaling of membranes with GRP and E-GRP

GRP spacer could be attributed to the electrostatic forces between the gypsum aggregation and membrane surface. For instance, collection of cations on polarized spacer surface could disrupt the gypsum formation on membrane surface because the electrostatic forces are well-known to effectively disperse gypsum aggregation.<sup>62</sup> Furthermore, some gypsum could also be attracted by the polarized spacer instead of blocking the membrane surface, as it is known from the literature that there is an enhanced ionic interaction between the negatively charged surfaces (E-GRP) and gypsum particles.<sup>63</sup> This was further supported by SEM images as less gypsum formation was observed for E-GRP compared to that of GRP (Figure 7).

Above, we discussed the advantages of using E-GRP for the enhancement of water flux, and prevention of membrane surface scaling. To make this approach more feasible in practical application, periodic polarization (or self-polarization) of spacers should be further investigated. One suggestion could be the use of E-GRP in self-polarizing systems by connecting external circuit. In addition, other types of fouling such as organic and biofouling should be also tested by considering larger scale applications.

At last, we shortly discuss about the cost of fabrication of E-GRP. The main cost comes from the electricity. Electricity costs from different countries for polarizing the spacer is given at (Figure S12a). For our case, we utilized 3 kW electricity per hour which costed us 0.678 dollars for 2 h. However, the other fabrication costs are relatively low. When we consider about the spacer material it is relatively low (0.057 dollars for 1 cm<sup>2</sup> spacer area). Furthermore, thanks to 3D printing, the fabrication did not require any labor price. Only the electricity cost of 3D printing which was 0.0027 dollars (for Korea) for 20 min of printing of our sample. Price calculation for different countries can be find at (Figure S12b).

## CONCLUSION

In this research, we propose a novel E-GRP spacer to maximize water flux and minimize gypsum scaling in FO application. The developed E-GRP has collected ions on itself and thereby enhanced local osmotic concentration near the membrane surface. When electrically polarized graphene blended polymer spacer E-GRP was used as draw spacer, it showed over 50%

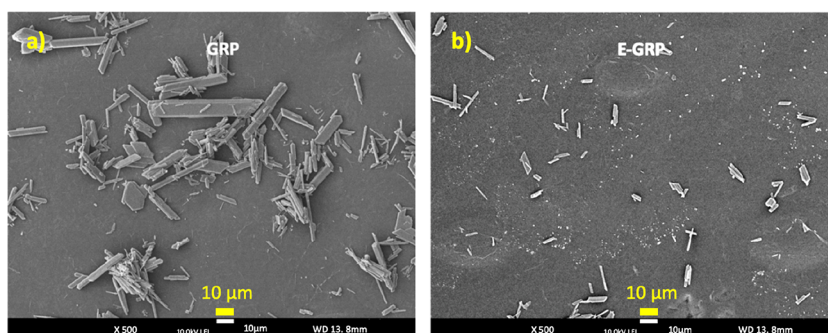


**Figure 7.** Gypsum scaled membranes of a) GRP and b) E-GRP.

higher water flux compared to the pristine nonconducting spacer (PLA) and graphene-blended spacer (GRP). When E-GRP was used as a feed spacer, it did not show highly enhanced performance due to the absence of ion present in the feed solution. However, when scaling test was performed by dissolving inorganic salts in feed side, E-GRP showed a great performance to mitigate membrane scaling by disrupting gypsum formation on membrane surface as result of collection of gypsum forming ions on spacer surface rather than membrane active layer and its effect on the dispersion of gypsum aggregation.

## ■ ASSOCIATED CONTENT

### Supporting Information

Supporting Information includes additional figures which may assist readers for further comprehension of the manuscript. It can be accessed online. Given figures in the Supporting Information are **Figure S1**. a) Cross-section and b) front views of the spacer designs (CAD models and illustrative drawings) **Figure S2**: a) Dipped membrane spacer-couples of GRP and E-GRP in 0.6 M NaCl solution, b) Designated membrane surface zones for measuring the concentrated salt amount: A1: membrane zone under the upper spacer filament (which has 0.635 mm intermembrane space under it), A2: membrane zone next to the spacer filament, A3: midzone between two spacer filaments (A2 = A3) **Figure S3**: Surface SEM images of graphene blended PLA spacers before (GRP) and after (E-GRP) electric polarization **Figure S4**. a) Cross-section and b) front views of the enhancement of the local osmotic concentration near surface of membrane to spacer **Figure S5**. Surface charge densities of the GRP and E-GRP samples in the 0.6 M NaCl solution **Figure S6**: Performances of PLA, GRP and E-GRP (Feed: DI Water, Draw: 3 M NaCl) **Figure S7**: Concentrated salt volumes on A1, A2 and A3 zones of membrane surfaces of. a) GRP, and b) E-GRP **Figure S8**: Surface profiles of A1, A2 and A3 zones of NaCl deposited membranes of a) GRP, and b) E-GRP (Red → blue: higher → lower concentration of NaCl) **Figure S9**: Water flux decline comparison of GRP and E-GRP for 10 h **Figure S10**. The PLA, GRP, and E-GRP spacers were submerged for 12 h in a 3 M NaCl solution to observe their ion absorption performance **Figure S11**. Surface charge densities of the GRP and E-GRP spacers in a 3 M NaCl solution **Figure S12**: a) Polarization cost of E-GRP for 2 h of polarization at 3 kW, b) Electricity cost for 20 min of 3D printing of graphene PLA filament through FDM type 3D printer (hot end at 205 °C and heated bed at 60 °C) The Supporting Information is available free of charge at <https://pubs.acs.org/doi/10.1021/acssuschemeng.0c09362>.

(PDF)

## ■ AUTHOR INFORMATION

### Corresponding Authors

**Heechul Choi** – School of Earth Sciences and Environmental Engineering, Gwangju Institute of Science and Technology (GIST), Gwangju, Republic of Korea; [orcid.org/0000-0002-8132-0983](https://orcid.org/0000-0002-8132-0983); Email: [hcchoi@gist.ac.kr](mailto:hcchoi@gist.ac.kr); Fax: +82-62-715-2423

**Moon Son** – School of Urban and Environmental Engineering, Ulsan National Institute of Science and Technology, Ulsan 44919, Republic of Korea; Phone: +82-62-715-2441; Email: [moonson619@unist.ac.kr](mailto:moonson619@unist.ac.kr)

### Authors

**Numan Yanar** – School of Earth Sciences and Environmental Engineering, Gwangju Institute of Science and Technology (GIST), Gwangju, Republic of Korea

**Eunmok Yang** – School of Earth Sciences and Environmental Engineering, Gwangju Institute of Science and Technology (GIST), Gwangju, Republic of Korea

**Hosik Park** – Green Carbon Research Center, Chemical Process Division, Korea Research Institute of Chemical Technology (KRICT), Daejeon 34114, Republic of Korea; [orcid.org/0000-0002-5151-1113](https://orcid.org/0000-0002-5151-1113)

Complete contact information is available at: <https://pubs.acs.org/doi/10.1021/acssuschemeng.0c09362>

### Notes

The authors declare no competing financial interest.

## ■ ACKNOWLEDGMENTS

This work was supported by National Research Foundation of Korea (NRF) projects funded by Korean Government (MSIT) with the grant numbers of No. 2020R1A2C2010808 and No. 2020M3H5A1081105.

## ■ REFERENCES

- (1) Mekonnen, M. M.; Hoekstra, A. Y. Four billion people facing severe water scarcity. *Sci. Adv.* **2016**, *2* (2), e1500323.
- (2) Okun, D. A. Water reclamation and nonpotable reuse: an option for meeting urban water supply needs. *Desalination* **1996**, *106* (1–3), 205–212.
- (3) Annalaura, C.; Ileana, F.; Dasheng, L.; Marco, V. Making waves: Coronavirus detection, presence and persistence in the water environment: State of the art and knowledge needs for public health. *Water Res.* **2020**, 115907.
- (4) Bhowmick, G. D.; Dhar, D.; Nath, D.; Ghangrekar, M. M.; Banerjee, R.; Das, S.; Chatterjee, J. Coronavirus disease 2019

(COVID-19) outbreak: some serious consequences with urban and rural water cycle. *npj Clean Water* **2020**, *3* (1), 1–8.

(5) La Rosa, G.; Bonadonna, L.; Lucentini, L.; Kenmoe, S.; Suffredini, E. Coronavirus in water environments: Occurrence, persistence and concentration methods-A scoping review. *Water Res.* **2020**, *179*, 115899.

(6) U. S. Environmental Protection Agency. Coronavirus and Drinking Water and Wastewater. <https://www.epa.gov/coronavirus/coronavirus-and-drinking-water-and-wastewater> (accessed 2020–09–21).

(7) Casanova, L.; Rutala, W. A.; Weber, D. J.; Sobsey, M. D. Survival of surrogate coronaviruses in water. *Water Res.* **2009**, *43* (7), 1893–1898.

(8) Naddeo, V.; Liu, H. Editorial Perspectives: 2019 novel coronavirus (SARS-CoV-2): what is its fate in urban water cycle and how can the water research community respond? *Environ. Sci. Water Res. Technol.* **2020**, *6* (5), 1213–1216.

(9) Fan, L.; Harris, J. L.; Roddick, F. A.; Booker, N. A. Influence of the characteristics of natural organic matter on the fouling of microfiltration membranes. *Water Res.* **2001**, *35* (18), 4455–4463.

(10) Nguyen, A. H.; Tobianson, J. E.; Howe, K. J. Fouling indices for low pressure hollow fiber membrane performance assessment. *Water Res.* **2011**, *45* (8), 2627–2637.

(11) Rastogi, N. K. Forward osmosis: Principles, applications, and recent developments. In *Current Trends and Future Developments on (Bio-) Membranes*; Elsevier: 2020; pp 3–35. DOI: 10.1016/B978-0-12-816777-9.00001-0.

(12) Abid, H. S.; Johnson, D. J.; Hashaikeh, R.; Hilal, N. A review of efforts to reduce membrane fouling by control of feed spacer characteristics. *Desalination* **2017**, *420*, 384–402.

(13) Ali, S. M.; Qamar, A.; Kerdi, S.; Phuntsho, S.; Vrouwenvelder, J. S.; Ghaffour, N.; Shon, H. K. Energy efficient 3D printed column type feed spacer for membrane filtration. *Water Res.* **2019**, *164*, 114961.

(14) Kerdi, S.; Qamar, A.; Vrouwenvelder, J. S.; Ghaffour, N. Fouling resilient perforated feed spacers for membrane filtration. *Water Res.* **2018**, *140*, 211–219.

(15) Siddiqui, A.; Farhat, N.; Bucs, S. S.; Linares, R. V.; Picioareanu, C.; Kruithof, J. C.; van Loosdrecht, M. C. M.; Kidwell, J.; Vrouwenvelder, J. S. Development and characterization of 3D-printed feed spacers for spiral wound membrane systems. *Water Res.* **2016**, *91*, 55–67.

(16) Yanar, N.; Kalleem, P.; Son, M.; Park, H.; Kang, S.; Choi, H. A New Era of Water Treatment Technologies: 3D Printing for Membranes *J. Ind. Eng. Chem.* **2020**, 911.

(17) Yanar, N.; Son, M.; Yang, E.; Kim, Y.; Park, H.; Nam, S.-E.; Choi, H. Investigation of the performance behavior of a forward osmosis membrane system using various feed spacer materials fabricated by 3D printing technique *Chemosphere* **2018**, 202708.

(18) Yang, H.-L.; Lin, J. C.-T.; Huang, C. Application of nanosilver surface modification to RO membrane and spacer for mitigating biofouling in seawater desalination. *Water Res.* **2009**, *43* (15), 3777–3786.

(19) Ronen, A.; Semiat, R.; Dosoretz, C. G. Impact of ZnO embedded feed spacer on biofilm development in membrane systems. *Water Res.* **2013**, *47* (17), 6628–6638.

(20) Ronen, A.; Lerman, S.; Ramon, G. Z.; Dosoretz, C. G. Experimental characterization and numerical simulation of the anti-biofouling activity of nanosilver-modified feed spacers in membrane filtration. *J. Membr. Sci.* **2015**, *475*, 320–329.

(21) An, J.; Cui, J.-F.; Zhu, Z.-Q.; Liang, W.-D.; Pei, C.-J.; Sun, H.-X.; Yang, B.-P.; Li, A. Conductive polymer-coated mesh films with tunable surface wettability for separation of oils and organics from water *J. Appl. Polym. Sci.* **2014**, *131* (18). DOI: 10.1016/j.jmemsci.2014.10.042.

(22) Sun, H.; Li, A.; Qin, X.; Zhu, Z.; Liang, W.; An, J.; La, P.; Deng, W. Three-Dimensional Superwetting Mesh Film Based On Graphene Assembly for Liquid Transportation and Selective Absorption. *ChemSusChem* **2013**, *6* (12), 2377–2381.

(23) Darmanin, T.; Guittard, F. Templateless electrodeposition of conducting polymer nanotubes on mesh substrates for high water adhesion. *Nano-Struct. Nano-Objects* **2016**, *7*, 64–68.

(24) Miller, D. J.; Araújo, P. A.; Correia, P. B.; Ramsey, M. M.; Kruithof, J. C.; van Loosdrecht, M. C. M.; Freeman, B. D.; Paul, D. R.; Whiteley, M.; Vrouwenvelder, J. S. Short-term adhesion and long-term biofouling testing of polydopamine and poly(ethylene glycol) surface modifications of membranes and feed spacers for biofouling control. *Water Res.* **2012**, *46* (12), 3737–3753.

(25) Araújo, P. A.; Miller, D. J.; Correia, P. B.; van Loosdrecht, M. C. M.; Kruithof, J. C.; Freeman, B. D.; Paul, D. R.; Vrouwenvelder, J. S. Impact of feed spacer and membrane modification by hydrophilic, bactericidal and biocidal coating on biofouling control. *Desalination* **2012**, *295*, 1–10.

(26) Yang, W.; Son, M.; Xiong, B.; Kumar, M.; Bucs, S.; Vrouwenvelder, J. S.; Logan, B. E. Effective Biofouling Control Using Periodic H<sub>2</sub>O<sub>2</sub> Cleaning with CuO Modified and Polypropylene Spacers. *ACS Sustain. Chem. Eng.* **2019**, *7* (10), 9582–9587.

(27) Abid, H. S.; Lalia, B. S.; Bertonecello, P.; Hashaikeh, R.; Clifford, B.; Gethin, D. T.; Hilal, N. Electrically conductive spacers for self-cleaning membrane surfaces via periodic electrolysis. *Desalination* **2017**, *416*, 16–23.

(28) Baek, Y.; Yoon, H.; Shim, S.; Choi, J.; Yoon, J. Electroconductive Feed Spacer as a Tool for Biofouling Control in a Membrane System for Water Treatment. *Environ. Sci. Technol. Lett.* **2014**, *1* (2), 179–184.

(29) Kim, S. J.; Ko, S. H.; Kang, K. H.; Han, J. Direct seawater desalination by ion concentration polarization. *Nat. Nanotechnol.* **2010**, *5* (4), 297–301.

(30) Son, M.; Kim, T.; Yang, W.; Gorski, C. A.; Logan, B. E. Electro-Forward Osmosis. *Environ. Sci. Technol.* **2019**, *53* (14), 8352–8361.

(31) Azamat, J. Functionalized Graphene Nanosheet as a Membrane for Water Desalination Using Applied Electric Fields: Insights from Molecular Dynamics Simulations. *J. Phys. Chem. C* **2016**, *120* (41), 23883–23891.

(32) Yanar, N.; Son, M.; Park, H.; Choi, H.; Yanar, N.; Son, M.; Park, H.; Choi, H. Toward greener membranes with 3D printing technology *Environ. Eng. Res.* **2020**, *26* (2). DOI: 10.4491/eeer.2020.027.

(33) Koo, J. W.; Ho, J. S.; An, J.; Zhang, Y.; Chua, C. K.; Chong, T. H. A Review on Spacers and Membranes: Conventional or Hybrid Additive Manufacturing? *Water Res.* **2021**, *188*, 116497.

(34) Kerdi, S.; Qamar, A.; Vrouwenvelder, J. S.; Ghaffour, N. Effect of localized hydrodynamics on biofilm attachment and growth in a cross-flow filtration channel. *Water Res.* **2021**, *188*, 116502.

(35) Carvalho Fernandes, D. C.; Lynch, D.; Berry, V. 3D-printed graphene/polymer structures for electron-tunneling based devices. *Sci. Rep.* **2020**, *10* (1), 11373.

(36) Foster, C. W.; Down, M. P.; Zhang, Y.; Ji, X.; Rowley-Neale, S. J.; Smith, G. C.; Kelly, P. J.; Banks, C. E. 3D Printed Graphene Based Energy Storage Devices. *Sci. Rep.* **2017**, *7* (1), 42233.

(37) Uyor, U. O.; Popoola, A. P.; Popoola, O.; Aigbodion, V. S. Energy storage and loss capacity of graphene-reinforced poly(vinylidene fluoride) nanocomposites from electrical and dielectric properties perspective: A review. *Adv. Polym. Technol.* **2018**, *37* (8), 2838–2858.

(38) Santos, E. J. G.; Kaxiras, E. Electric-Field Dependence of the Effective Dielectric Constant in Graphene. *Nano Lett.* **2013**, *13* (3), 898–902.

(39) Nakagawa, T.; Nakiri, T.; Hosoya, R.; Tajitsu, Y. In *Electrical properties of biodegradable polylactic acid film, Proceedings of the 7th International Conference on Properties and Applications of Dielectric Materials (Cat. No.03CH37417)*, 1–5 June 2003; 2003; pp 499–502 vol.2.

(40) Yanar, N.; Son, M.; Park, H.; Choi, H. Bio-mimetically inspired 3D-printed honeycombed support (spacer) for the reduction of reverse solute flux and fouling of osmotic energy driven membranes. *J. Ind. Eng. Chem.* **2020**, *83*, 343–350.

- (41) Hu, J.; Liang, C.; Han, C.; Zhou, Q.; Ma, J.; Liu, D.; Chen, X. Effect of external electric field on particle impact charging process. *Powder Technol.* **2020**, *360*, 1355–1367.
- (42) Yang, F.; Wu, W.; Chen, S.; Gan, W. The ionic strength dependent zeta potential at the surface of hexadecane droplets in water and the corresponding interfacial adsorption of surfactants. *Soft Matter* **2017**, *13* (3), 638–646.
- (43) Britannica, The Eds. of Encyclopaedia. Dielectric constant. Encyclopedia Britannica. <https://www.britannica.com/science/dielectric-constant> (accessed 2020–10–26).
- (44) Hasted, J. B.; Ritson, D. M.; Collie, C. H., Dielectric Properties of Aqueous Ionic Solutions. Parts I and II. *J. Chem. Phys.* **1948**, *16* (1), 1–21.
- (45) Smith, A. M.; Lee, A. A.; Perkin, S. The Electrostatic Screening Length in Concentrated Electrolytes Increases with Concentration. *J. Phys. Chem. Lett.* **2016**, *7* (12), 2157–2163.
- (46) Alayande, A. B.; Obaid, M.; Yu, H.-W.; Kim, I. S. High-flux ultrafiltration membrane with open porous hydrophilic structure using dual pore formers. *Chemosphere* **2019**, *227*, 662–669.
- (47) Park, S.; Yang, E.; Park, H.; Choi, H. Fabrication of functionalized halloysite nanotube blended ultrafiltration membranes for high flux and fouling resistance. *Environ. Eng. Res.* **2020**, *25* (5), 771–778.
- (48) Nguyen, H. T.; Nguyen, N. C.; Chen, S.-S.; Li, C.-W.; Hsu, H.-T.; Wu, S.-Y. Innovation in Draw Solute for Practical Zero Salt Reverse in Forward Osmosis Desalination. *Ind. Eng. Chem. Res.* **2015**, *54* (23), 6067–6074.
- (49) Mi, B.; Elimelech, M. Gypsum Scaling and Cleaning in Forward Osmosis: Measurements and Mechanisms. *Environ. Sci. Technol.* **2010**, *44* (6), 2022–2028.
- (50) Wang, J.; Wang, L.; Miao, R.; Lv, Y.; Wang, X.; Meng, X.; Yang, R.; Zhang, X. Enhanced gypsum scaling by organic fouling layer on nanofiltration membrane: Characteristics and mechanisms. *Water Res.* **2016**, *91*, 203–213.
- (51) Al-Mutaz, I. S.; Al-Ghunaimi, M. A. In Performance of reverse osmosis units at high temperatures. *The IDA World Congress on Desalination and Water Reuse*, IDA, Bahrain, 2001.
- (52) Persson, R. A. X. On the dielectric decrement of electrolyte solutions: a dressed-ion theory analysis. *Phys. Chem. Chem. Phys.* **2017**, *19* (3), 1982–1987.
- (53) Topping, C. What is the cheapest electricity in the world? Electricity prices by country. <https://www.ovoenergy.com/guides/energy-guides/average-electricity-prices-kwh.html> (accessed 2021–02–27).
- (54) U. S. Energy Information Administration, Average Price of Electricity to Ultimate Customers by End-Use Sector. 2021. [https://www.eia.gov/electricity/monthly/epm\\_table\\_grapher.php?t=epmt\\_5\\_6\\_a](https://www.eia.gov/electricity/monthly/epm_table_grapher.php?t=epmt_5_6_a) (accessed 2021–02–27).
- (55) The World Bank Group, Gross domestic product 2019. <https://datacatalog.worldbank.org/dataset/gdp-ranking> (accessed 2021–02–28).
- (56) 3D Printerly, How Much Electric Power Does a 3D Printer Use? <https://3dprinterly.com/how-much-electric-power-does-a-3d-printer-use/> (accessed 2021–02–28).
- (57) Elimelech, M.; Gregory, J.; Jia, X.; Williams, R. A., Chapter 2 - Electrical properties of interfaces. In *Particle Deposition & Aggregation*, Elimelech, M.; Gregory, J.; Jia, X.; Williams, R. A., Eds. Butterworth-Heinemann: Woburn, 1995; pp 9–32.
- (58) Yangali-Quintanilla, V.; Li, Z.; Valladares, R.; Li, Q.; Amy, G. Indirect desalination of Red Sea water with forward osmosis and low pressure reverse osmosis for water reuse. *Desalination* **2011**, *280* (1), 160–166.
- (59) Pal, P., Chapter 5 - Water Treatment by Membrane-Separation Technology. In *Industrial Water Treatment Process Technology*, Pal, P., Ed. Butterworth-Heinemann: 2017; pp 173–242.
- (60) Conway, B. E.; Bockris, J. M.; Ammar, I. A. The dielectric constant of the solution in the diffuse and Helmholtz double layers at a charged interface in aqueous solution. *Trans. Faraday Soc.* **1951**, *47*, 756–766.
- (61) Philpott, M. R.; Glosli, J. N. Screening of Charged Electrodes in Aqueous Electrolytes. *J. Electrochem. Soc.* **1995**, *142* (2), L25–L28.
- (62) Cheng, H.; Wang, N.; Song, H.; Cheng, F. Effect of calcium sulfate dehydrate and external electric field on the sedimentation of fine insoluble particles. *Desalination Water Treat.* **2016**, *57* (1), 335–344.
- (63) Chen, S. C.; Su, J.; Fu, F.-J.; Mi, B.; Chung, T.-S. Gypsum (CaSO<sub>4</sub>·2H<sub>2</sub>O) Scaling on Polybenzimidazole and Cellulose Acetate Hollow Fiber Membranes under Forward Osmosis. *Membranes* **2013**, *3* (4), 354–374.